Science of the Total Environment 795 (2021) 148854

Contents lists available at ScienceDirect

Science of the Total Environment

journal homepage: www.elsevier.com/locate/scitotenv

Functional dynamics of vegetated model patches: The minimum patch size effect for canopy restoration

Aina Barcelona [a,*], Carolyn Oldham [b], Jordi Colomer [a], Teresa Serra [a]

[a] Department of Physics, University of Girona, 17071 Girona, Spain
[b] School of Engineering, The University of Western Australia, Perth, WA 6009, Australia

HIGHLIGHTS

- A minimum seagrass patch size is needed for successful canopy restoration
- The response of seagrass patches depends on wave velocity and canopy density.
- Under low velocities seagrasses do not interact with waves, but attenuate seabed *TKE*.
- Under moderate to high wave velocities seagrasses interact with waves producing *TKE*.

GRAPHICAL ABSTRACT

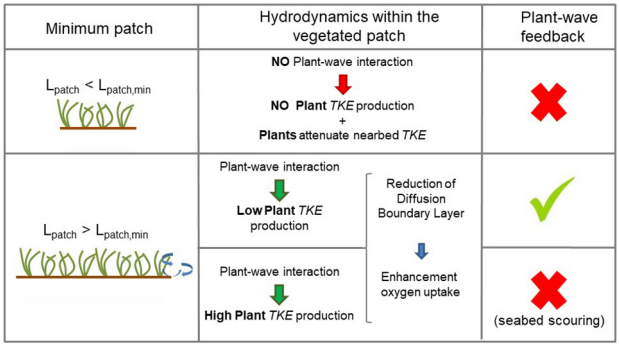

ARTICLE INFO

Article history:
Received 30 January 2021
Received in revised form 31 May 2021
Accepted 30 June 2021
Available online 3 July 2021

Editor: Martin Drews

Keywords:
Seagrass patch length
Turbulent kinetic energy
Wave velocity
Canopy density

ABSTRACT

For the past two centuries coastal zones have been suffering seagrass loss resulting in a network of vegetated patches which are barely interconnected and which may compromise the ecological services provided by the canopy. To optimize management efforts for successful restoration strategies, questions need to be addressed about what appropriate canopy architectural considerations are required under certain hydrodynamic conditions. In this study, a set of laboratory experiments were conducted in which hydrodynamic conditions, plant densities and vegetated patch lengths were varied to determine minimum patch lengths for successful management strategies. Based on the *TKE* production, this study finds two possible canopy behaviours of seagrasses under oscillating flows: one where plants do not interact with the flow and the other where they interact with waves and produce *TKE*. A threshold from the first to second behaviour occurs for $[C_{D-Patch}\frac{nd^2}{2(1-\phi)}]^{\frac{1}{3}}U_w = 2$, where C_D is the drag of the vegetated patch, n is the number of stems per m^2, d is the stem diameter and ϕ is the solid plant fraction. Therefore, high canopy densities, large patches of vegetation or moderate wave velocities will produce plant-wave interaction, whereas low canopy densities, small vegetation patches or slow wave velocities will produce a behaviour akin to the non-vegetated cases.
© 2021 The Authors. Published by Elsevier B.V. This is an open access article under the CC BY-NC-ND license (http://creativecommons.org/licenses/by-nc-nd/4.0/).

1. Introduction

Seagrass meadows are seascape ecosystems providing key ecological services in coastal areas such as providing habitats for thousands of fish, bird and invertebrate species (Hughes et al., 2009), supporting commercial fisheries (Metz et al., 2020), regulating nutrient cycling (Montefalcone, 2009), stabilizing seabed sediments (Bouma et al., 2007; Waycott et al., 2009) and mitigating climate change through both carbon storage and sequestration (Fourqurean et al., 2012; Unsworth et al., 2018).

Seagrasses are found in shallow coastal waters (most less than 10 m deep), making them vulnerable to human pressure which can cause direct physical damage to the meadow itself through anchoring, trawling,

* Corresponding author.
E-mail address: aina.barcelona@udg.edu (A. Barcelona).

https://doi.org/10.1016/j.scitotenv.2021.148854
0048-9697/© 2021 The Authors. Published by Elsevier B.V. This is an open access article under the CC BY-NC-ND license (http://creativecommons.org/licenses/by-nc-nd/4.0/).

dredging or urban/port infrastructure development, or indirect damage through nutrient over-enriched waters and/or high sediment loads coming from urban/industrial runoff, aquaculture, and agricultural runoff (Abadie et al., 2016; Grech et al., 2012; Montefalcone, 2009). Consequently, almost 15% of seagrass species worldwide are threatened (Hughes et al., 2009). Waycott et al. (2009) reported that since 1879, 29% of the world's seagrasses have been lost. Furthermore, since 1980 seagrass meadows have disappeared at a rate of 110 km^2 yr^{-1} which, in turn, results in sea soil remineralization and consequently a stock carbon release of up to 299 Tg C yr^{-1} (Fourqurean et al., 2012). Some of the less affected seagrass canopies end with gaps within vegetation patches, contributing to the meadow heterogeneity, while the most endangered seagrass canopies end up as a group of interconnected patches (Sleeman et al., 2005).

Seagrass loss is presented either by an increase in habitat fragmentation that transforms a continuous tract of vegetation into canopies with interspersed gaps (i.e., areas of bare soil interspersed within the meadow) or by a network of vegetated patches in which interconnections are compromised (Robbins and Bell, 1994; Tanner, 2003). Compared with continuous canopies and given their difficulties in coping with hydrodynamical stressors, vegetation patches are usually described as having lower plant densities, shorter leaves and lower nutrient storage (Gera et al., 2013). The functional dynamics of seagrass canopies depend on attenuating the wave velocity (Newell and Koch, 2004) and the turbulent kinetic energy (*TKE*) (Pujol et al., 2013a) which both hinge on plant density and flexibility and the submergence ratio and distance from the meadow edge. As such, the ecological services of fragmented seagrass canopies are expected to be compromised (Paul and Amos, 2011; Serra et al., 2018) because fragmented seagrasses are not fully able to reduce the energy of the flow and therefore the sheltering effect of vegetation is reduced (El Allaoui et al., 2016). Not only this, as the increase in seagrass fragmentation will result in an increase in edges over the canopy areas then the attenuation of the hydrodynamics is also reduced (Granata et al., 2001). Edges are transitional areas between the bare soil and the canopy and represent transition zones for local hydrodynamics. They are mainly a region of the canopy with low wave velocity and *TKE* attenuation compared to a bare bed and where both wave velocity and *TKE* decrease gradually towards the inner canopy region (Serra et al., 2018).

Most studies have focused on the patch size effect on unidirectional flows to discern the structural characteristic of patches and their role in optimising the ecological services provided. For instance, Licci et al. (2019) evaluated the effects of patches of *Callitriche platycarpa* Kütz in lotic ecosystems and found that small patches induced little to no modification to physical parameters. Patches, however, as noted by Folkard (2005), can significantly modify hydrodynamic patterns depending on the distance between them. Likewise, Li et al. (2019) found that vegetated patches greatly impacted the downstream flow: the greater the plant density was, the lower the depth-averaged velocity adjacent to the patch. Concurrent with these results but under oscillatory wave conditions, El Allaoui et al. (2016) found that at the edges of vegetation the sheltering provided was reduced compared to within the canopy, although denser fragmented canopies produced greater sheltering than sparser ones did. The structural characteristics, such as plant density and leaf length, of *Posidonia oceanica* (Linnaeus) Delile meadows determine flow attenuation, with vegetation sheltering nearby gaps (depending on the length of the gaps) in such a way that larger gaps were less protected by the nearby canopy (Colomer et al., 2017). Therefore, fragmented seagrasses that undergo patchiness result in more vulnerable meadows that are then exposed to higher levels of energy which may amplify sediment resuspension and turbidity and produce negative feedback on the canopies (Zhang et al., 2018; Carr et al., 2010).

All of these results have strong implications for seagrass ecosystem restoration strategies which are designed to recover seascapes, their ecosystem biodiversity and the services they provide (Gilby et al., 2020; van Katwijk et al., 2016). Although the first trials for seagrass restoration started during the first half of the twentieth century, it was not until 1970 that interest in restoring seagrass ecosystems increased (van Katwijk et al., 2016). Furthermore, the increased effect that anthropogenic emissions and activities have on the fate of fragmented canopies has meant there is an urgent need to restore world's seascapes, among which include seagrass canopies. Some studies have also modelled seagrass restoration efficiency using chemical and physical abiotic variables such as light, temperature and salinity (Stankovic et al., 2019). For successful restorations, strategies such as improving water quality, removing exotic species, and ensuring the minimum number of shoots planted is within the range of 1000–10,000 shoots/seeds have been implemented (Kupsky and Dornbush, 2019). Many attempts to transplant plants into fragmented canopies have resulted in limited survival rates varying from 9% to 40% according to Paling et al. (2003), while van Katwijk et al. (2016) found that the survival rate was estimated at 37% for the majority of the seagrass restoration trials. Such results indicate the importance of establishing functional dynamic criteria for the patch length scales required if plants are to be successfully replanted in the canopies. Infantes et al. (2009) indicated that high wave velocities produce a loss in the *Posidonia oceanica*' cover. Therefore, despite all the studies carried out, none of them focus on the functional dynamics of the patch, which is dependent on the patch scale; therefore there is a need to include hydrodynamics in the parametrization for future projects of plant restoration.

This study, then, is focused on determining whether there is (or not) an optimal patch length in which the hydrodynamics of the patch mimics those of a canopy without fragmentation. The objective of this study is to determine whether (or not) a single patch behaves dynamically as a canopy. As such, the minimum patch size was defined as the critical length over which a single patch was dynamically mimicking a continuous canopy under a certain oscillatory flow regime. It is expected that a patch with functional dynamics akin to those of a canopy might be optimal for successful replantation. Thus, different patches with different lengths and vegetation densities were combined to obtain the structural scale that can guarantee successful seagrass canopy restoration.

2. Methodology

2.1. The flume

The study was carried out in a laboratory methacrylate flume (600 cm long, 50 cm wide and 60 cm deep, Fig. 1) with a mean water height of $h = 30$ cm (Table 1). The flume was equipped with a vertical paddle-type wavemaker at the entrance. The wavemaker was driven by a variable-speed motor at two frequencies ($f = 0.50$, 1.12 Hz). A plywood beach (slope = 1:2) covered with foam rubber to eliminate wave reflection was placed at the end of the flume (Pujol et al., 2013a; Serra et al., 2018). At the measurement depth, the percentage of U_c reduction was 39% and 59% for the wave frequencies of 1.12 Hz and 0.5 Hz, respectively. There was also a reduction of 3.0% and 2.9% for the wave velocity for frequencies of 1.12 Hz and 0.5 Hz, respectively. In the longitudinal direction, $x = 0$ cm was situated at the wavemaker, in the lateral direction, $y = 0$ cm was at the centre of the tank, and in the vertical direction, $z = 0$ cm was situated at the flume bed.

2.2. Patches of flexible vegetation

The system of laboratory model vegetation consisted of a series of flexible plants made from eight 0.075 mm thick polyethylene canopy blades attached to PVC dowels that had been randomly inserted into a perforated baseboard ($L_{base\text{-board}} = 250$ cm, Pujol et al., 2013a), with a rigid dowel extending 1 cm above the bed (Zhang et al., 2018). The model plants were geometrically and dynamically similar to *Posidonia oceanica* plants (Ghisalberti and Nepf, 2002; Pujol et al., 2013a). The leaf length was 14 cm, and the effective height when the leaves were

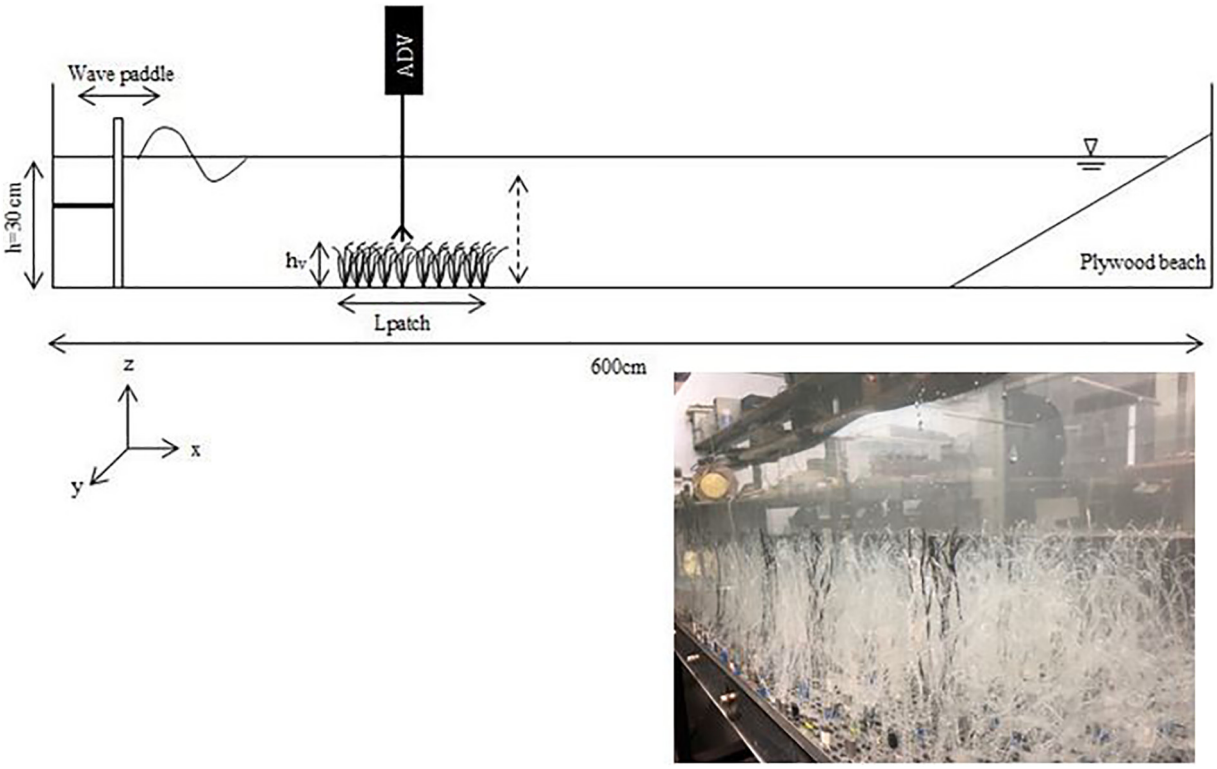

Fig. 1. A lateral view of the experimental setup (top), with the wave paddle on the left to provide waves from left to right. Experiments were conducted in a 600x50x50 cm long flume, with a mean water depth of 30 cm. The model patch had patch lengths that ranged from 2.8 cm to 42 cm. The triangle at the water-air interface represents the water level in the flume. An ADV was vertically mounted to measure the instantaneous velocities at selected vertical heights. A photograph of the experimental setup (bottom), with the simulated vegetation.

bent by the waves was $h_v = 8.5$ cm for $f = 1.12$ Hz and $h_v = 10.5$ cm for $f = 0.5$ Hz. The effective heights were calculated by the mean between both the maximum and the minimum bending heights of the plants for 25 oscillations The initial position of the vegetation (x_0) was situated 100 cm from the wavemaker (Fig. 1). The vegetation density of patches was quantified using the solid plant fraction (*SPF*) defined as:

$$\mathrm{SPF}\ (\%) = 100n\pi\left(\frac{d}{2}\right)^2 \quad (1)$$

where n is the number of stems per unit area and d is the stem diameter (1 cm). Six *SPF*s were used (0%, 2.5%, 3.5%, 5%, 7.5% and 10%), which corresponded to vegetation densities of $n = 0$, 318, 446, 637, 955 and 1273 stems·m^{-2} (Fig. 2) and similar to the canopy densities between 78 to 1000 stems·m^{-2} found in coastal areas (Bacci et al., 2017; Colomer et al., 2017; Gera et al., 2013; van Katwijk et al., 2010); *SPF* = 0% corresponded to the case with no vegetation. For each *SPF*, different patch sizes, L_{patch}, ranging from 32 to 240 cm were considered (Table 2). In this study, the longest patch $L_{patch} = 240$ cm. A total of 67 experiments were performed for the different *SPF*s, patch lengths and wave frequencies (Table 2). In the experiments, the patch edge was considered as the interface from the vegetated region and the non-vegetated region (Schoelynck et al., 2018). For all patch lengths, flow velocity profiles were measured at the centre of the patch. The length of the patch increased from this centre point outwards (i.e., to the wave maker and to the beach, see Fig. 1) so that the measuring point was always the same for all patches.

Table 1
Nomenclature table.

Variable	Units	Definition
a	cm^2	Frontal area
A_w	cm	Wave excursion length
A_w/S_b	Non-dimensional	Ratio between wave excursion to plant-to-plant distance between blades
f	Hz	Wave frequency
h	cm	Water height
h_v	cm	Effective plant height
L	cm	Vegetation length
L_{canopy}	cm	Canopy length
L_{patch}	cm	Patch length
n	stems·m^{-2}	Canopy density
n_b	Blades	Blade density
S_b	cm	Plant-to-plant distance between blades
SPF	%	Solid plant fraction
TKE	cm^2·s^{-2}	Turbulent kinetic energy
u	cm·s^{-1}	Eulerian velocity in the x direction
u'	cm·s^{-1}	Turbulent velocity
U_c	cm·s^{-1}	Steady velocity associated with the current
U_i	cm·s^{-1}	Instantaneous velocity
$U_i(\varphi)$	cm·s^{-1}	Instantaneous velocity according to the phase
U_w	cm·s^{-1}	Wave velocity
U_w^{rms}	cm·s^{-1}	Orbital velocity
v	cm·s^{-1}	Eulerian velocity in the y direction
w	cm·s^{-1}	Eulerian velocity in the z direction
x	cm	Longitudinal direction
$x = 0$	cm	Position of the wave paddle
y	cm	Lateral direction
z	cm	Vertical direction
α_w	Non-dimensional	Ratio of vegetated to non-vegetated U_w
β_w	Non-dimensional	Ratio of vegetated to non-vegetated *TKE*
φ	Radians	Wave phase
ϕ	Non-dimensional	Solid plant fraction

2.3. Measuring velocities

The Eulerian velocity field was defined as (u, v, w) in the (x, y, z) directions, respectively. The three components of velocity were recorded (50 Hz over 5 min) with a downwards looking Acoustic Doppler Velocimeter (16-MHz MicroADV, Sontek). The ADV measured at a distance of 5 cm from the probe tip and with a sampling volume of 0.09 cm^3. Beam correlations less than 70% were discarded and spikes were removed (Goring and Nikora, 2002; Pujol et al., 2013a). The longitudinal

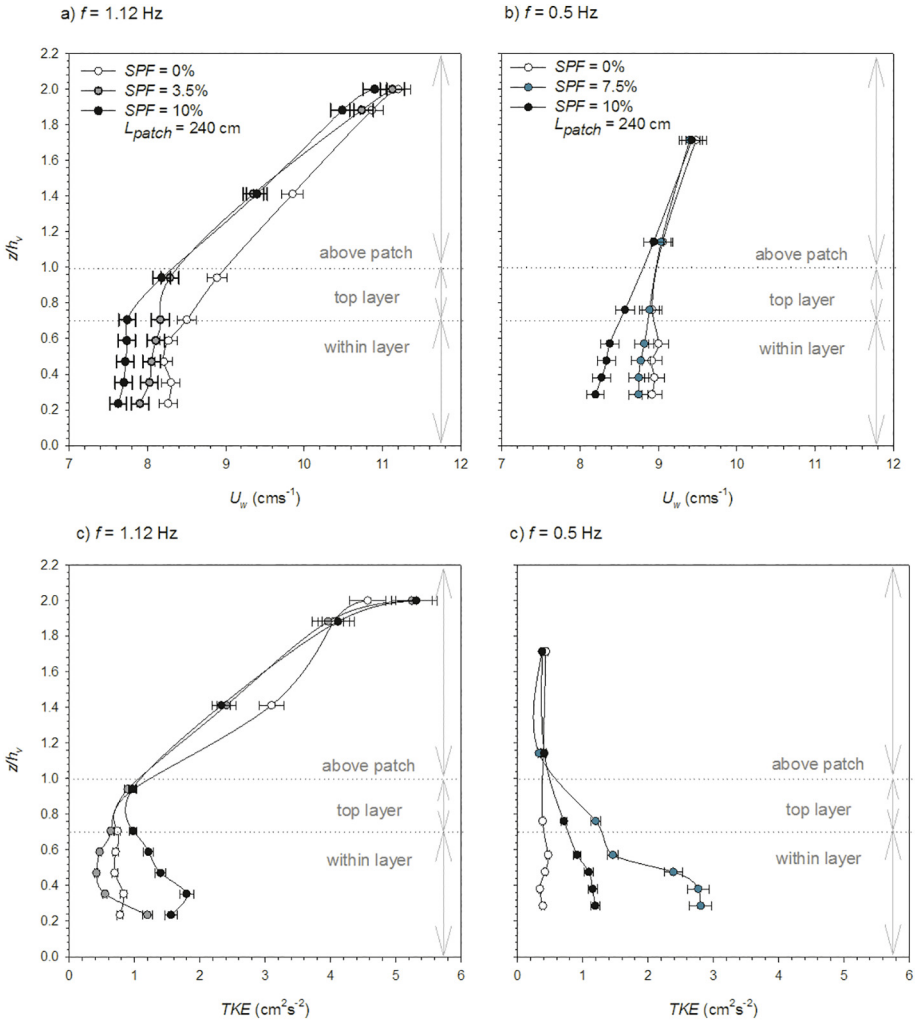

Fig. 2. Wave velocity (U_w) vertical profiles for a) $f = 1.12$ Hz, b) $f = 0.5$ Hz and *TKE* vertical profiles for c) $f = 1.12$ Hz and d) $f = 0.5$ Hz. Unfilled circles correspond to the cases of $SPF = 0\%$, whereas black, blue and grey filled symbols correspond to $SPF = 10\%$, 7.5%, and 3.5% respectively. The experiments presented here correspond to the $L_{patch} = 240$ cm patch length case.

velocity was measured at an antinode to eliminate the lower order spatially periodic variation in wave and velocity amplitude associated with wave reflection (Luhar et al., 2010; Pujol et al., 2013a). The ADV was mounted on a movable vertical frame (at y = 0 cm, Fig. 1) and manually adjusted to measure a vertical profile. Some plants were removed to avoid blocking the ADV beams (Ros et al., 2014; Zhang et al., 2018), and were re-inserted into nearby holes.

2.4. Hydrodynamic analysis

For oscillatory flows, the instantaneous velocity in the *x* direction, $U_i(t)$, can be decomposed as:

$$U_i(t) = U_c + U_w + u' \tag{2}$$

where U_c is the steady velocity associated with the wave, U_w is the unsteady wave motion in the *x* direction which represents spatial variations in the phase-averaged velocity field, and u' is the turbulent velocity, that is, the instantaneous velocity fluctuation in the x-direction. U_c is the phase-averaged velocity:

$$U_c = \frac{1}{2\pi}\int_0^{2\pi} U_i(\varphi)\partial\varphi \tag{3}$$

where $U_i(\varphi)$ is the instantaneous velocity according to the phase (Lowe et al., 2005; Luhar et al., 2010). Wave velocity, U_w, was obtained by using a phase averaging technique. The Hilbert transform was used to average oscillatory flow velocities with a common phase (Pujol et al., 2013b; Ros et al., 2014). The root mean square (rms) of $U_i(\varphi)$ was considered as the characteristic value of the orbital velocity U_w^{rms} (U_w hereafter) at each depth and was calculated according to:

$$U_w^{rms} = \sqrt{\frac{1}{2\pi}\int_0^{2\pi} (U_i(\varphi) - U_c)^2 \partial\varphi} \tag{4}$$

The ratio α_w of the wave velocity (U_w) was calculated following Lowe et al. (2005):

$$\alpha_w = \frac{U_w}{U_{w,WP}} \tag{5}$$

where U_w is the wave velocity within the patch at z = 4 cm for vegetated cases and $U_{w,WP}$ is the wave velocity at z = 4 cm for non-vegetated cases. The measurements within the vegetation at $z = 4$ cm corresponded to $z/h_v = 0.47$ for $f = 1.12$ Hz and $z/h_v = 0.38$ for $f = 0.5$ Hz. This depth was chosen from the wave velocity profile, shown later on in the results section so that it was situated out of the shear region situated at the top of the vegetation and also far from the bed of the flume. Therefore, α_w provided a measure of the wave velocity attenuation within the patch for vegetated cases compared to non-vegetated cases. Consequently, values of $\alpha_w \approx 1$ indicated a weak or negligible

Table 2
Summary of the experiment characteristics.

Run	f (Hz)	SPF (%)	n (stems·m^{-2})	L_{patch} (cm)	aL	Aw/S_b	Run	f (Hz)	SPF (%)	n (stems·m^{-2})	L_{patch} (cm)	aL	Aw/S_b
WP1	0.5	0	0		0		SFV34	1.12	3.5	446	70	3.12	0.70
WP2	1.12	0	0		0		SFV35				112	5.00	0.69
SFV3	0.5	1	127	42	0.53	0.94	SFV36				126	5.62	0.69
SFV4				70	0.89	0.92	SFV37				140	6.24	0.70
SFV5				112	1.42	0.92	SFV38				154	6.87	0.68
SFV6				196	2.49	0.94	SFV39				168	7.49	0.68
SFV7		7.5	955	42	4.01	2.84	SFV40				196	8.74	0.68
SFV8				70	6.69	2.75	SFV41				240	10.61	0.67
SFV9				112	10.70	2.77	SFV42		5	637	42	2.68	0.83
SFV10				196	18.72	2.67	SFV43				70	4.46	0.83
SFV11		10	1273	42	5.35	3.11	SFV44				98	6.24	0.83
SFV12				70	8.91	3.08	SFV45				126	8.03	0.82
SFV13				84	10.69	2.97	SFV46				168	12.49	0.80
SFV14				98	12.48	2.96	SFV47				196	10.70	0.81
SFV15				112	14.26	2.92	SFV48				210	13.38	0.80
SFV16				133	16.93	2.98	SFV49				240	15.16	0.80
SFV17				140	17.82	2.84	SFV50		7.5	955	42	4.01	1.03
SFV18				154	19.60	2.97	SFV51				70	6.69	1.04
SFV19				182	23.17	3.04	SFV52				84	8.02	1.01
SFV20				224	28.52	2.89	SFV53				98	9.36	1.01
SFV21				240	30.30	2.86	SFV54				112	10.70	0.99
SFV22	1.12	2.5	318	42	1.34	0.59	SFV55				133	12.03	0.98
SFV23				70	2.23	0.60	SFV56				154	14.71	0.99
SFV24				84	2.67	0.59	SFV57				196	18.72	0.96
SFV25				98	3.12	0.59	SFV58				240	22.73	0.97
SFV26				112	3.56	0.58	SFV59		10	1273	42	5.35	1.18
SFV27				126	4.01	0.59	SFV60				70	8.91	1.18
SFV28				140	4.45	0.59	SFV61				84	10.69	1.15
SFV29				154	4.90	0.59	SFV62				98	12.48	1.15
SFV30				168	5.34	0.59	SFV63				112	16.04	1.13
SFV31				182	5.79	0.59	SFV64				133	24.95	1.10
SFV32				196	6.23	0.59	SFV65				168	19.60	1.12
SFV33				240	7.57	0.59	SFV66				196	21.39	1.12
							SFV67				240	30.30	1.11

attenuation of the wave velocity by the vegetation, whereas low values of $\alpha_w < 1$ indicated high wave velocity attenuation.

The turbulent velocity was obtained by:

$$u' = U_i - U_c - U_w \tag{6}$$

where U_c and U_w were calculated by Eqs. 3 and 4. The turbulent velocity was calculated for all directions (u', v' and w') for z = 4 cm.

Turbulent kinetic energy (TKE) was calculated following Ros et al. (2014) as:

$$TKE = \frac{1}{2}\left(\left\langle u'^2\right\rangle + \left\langle v'^2\right\rangle + \left\langle w'^2\right\rangle\right) \tag{7}$$

where $< >$ denotes the time average.

The ratio, β_w, was calculated following Colomer et al. (2017):

$$\beta_w = \frac{TKE}{TKE_{WP}} \tag{8}$$

where TKE was the turbulent kinetic energy within the patch at z = 4 cm for vegetated cases and TKE_{WP} was the TKE measured at z = 4 cm for the non-vegetated case. Therefore, values of $\beta_w \approx 1$ indicated a weak or negligible attenuation of the TKE, whereas low values of $\beta_w < 1$ indicated a high TKE attenuation compared to the non-vegetated case.

In order to gain knowledge of the vertical distribution of TKE within the patch, a non-dimensional model was set following Zhang et al. (2018). For a full canopy, Zhang et al. (2018) found that the relationship between the TKE, U_w and the main canopy parameters followed:

$$\frac{\sqrt{TKE}}{U_w} = \delta\left[C_D \frac{l_t}{d}\frac{nd}{2(1-\phi)}\right]^{\frac{1}{3}} \tag{9}$$

where δ is the scale constant, ϕ is the solid volume fraction, $\phi = n\frac{\pi}{4}d^2$, l_t is characteristic eddy length-scale, and C_D is the drag of the form of the obstacle along the fluid patch, with $C_D = 1.4$ being used in both studies. In Eq. (9), the characteristic length scale, L_{patch} / L_{canopy}, for each frequency, is introduced to account for the volume of the patch in relation to the maximum canopy volume in the form of $\frac{V_{Patch}^{1/3}}{V_{Canopy}^{1/3}} = \left(\frac{aL_{patch}}{aL_{canopy}}\right)^{\frac{1}{3}} = \left(\frac{L_{patch}}{L_{canopy}}\right)^{\frac{1}{3}}$, therefore Eq. (9) is expressed following:

$$\frac{\sqrt{TKE}}{U_w} = \delta\left[C_D\left(\frac{L_{patch}}{L_{canopy}}\right)^{\frac{1}{3}}\frac{l_t}{d}\frac{nd^2}{2(1-\phi)}\right]^{\frac{1}{3}} \tag{10}$$

Zhang et al. (2018) considered $l_t = d$ for $S > 2d$ whereas $l_t = S$ for $S < 2d$. In the present study, since $S > 2d$, $l_t = d$, therefore:

$$\frac{\sqrt{TKE}}{U_w} = \delta\left[C_D\left(\frac{L_{patch}}{L_{canopy}}\right)^{\frac{1}{3}}\frac{nd^2}{2(1-\phi)}\right]^{\frac{1}{3}} \tag{11}$$

Defining $C_{D\text{-}Patch} = C_D(L_{patch}/L_{canopy})^{1/3}$ as the drag generated by the patch, Eq. (11) results:

$$\frac{\sqrt{TKE}}{U_w} = \delta\left[C_{D-Patch}\frac{nd^2}{2(1-\phi)}\right]^{\frac{1}{3}} \tag{12}$$

3. Results

For the longest patch considered (L_{patch} = 240 cm), the wave velocity U_w decreased with depth for all the experiments i.e., with and without plants (Fig. 2). Three vertical layers could be differentiated based on the vertical profile of U_w. A first layer above the patch ($z/h_v > 1$), where U_w for the vegetated case was similar to that of the without-plants case. A second layer within the patch ($0.7 < z/h_v < 1$), where U_w for the case with plants was lower than that for the non-vegetated case and decreased gradually with depth. A third layer within the patch, the inner vegetation layer ($z/h_v < 0.7$), where U_w was nearly constant with depth down to the bed. The vertical decrease of U_w for the higher frequency case (1.12 Hz) was stronger than for the low frequency (0.5 Hz) (Fig. 2a and b). For the higher frequency, a decrease in the U_w from the lowest to greatest depth was found for all the vegetated and non-vegetated cases (Fig. 2a), while for the lower frequency, U_w presented the slowest vertical reduction, especially for the non-vegetated cases (Fig. 2b). For the non-vegetated cases and for the high frequency, *TKE* decreased with depth down to $z/h_v = 0.7$. Below $z/h_v = 0.7$, the *TKE* remained constant down to the bed (Fig. 2c). In contrast, for the low frequency in non-vegetated cases, *TKE* was constant with depth (Fig. 2d). Unlike what had been obtained for U_w, the *TKE* was higher for vegetated than for non-vegetated cases, except for *SPF* = 3.5% at the higher frequency (Fig. 2c and d). For the higher frequency and the vegetated and non-vegetated cases, the *TKE* decreased with depth. However, for the vegetated cases, the *TKE* slightly increased with depth from $z/h_v =$ 0.7 down to the bed (Fig. 2c).

Both wave attenuation (α_w) and *TKE* attenuation (β_w) were calculated for the different non-dimensional patch length scales (L_{patch}/h_v) and for the different *SPF*s studied (Fig. 3). For both frequencies, the greater the *SPF* was, the lower α_w was (Fig. 3a and b). For the high frequency studied (f = 1.2 Hz) and for *SPF* = 2.5%, α_w remained constant with L_{patch}/h_v (Fig. 3a). For the other *SPF* studied (>2.5%), α_w was constant for low L_{patch}/h_v decreasing afterward as L_{patch}/h_v increased. Therefore, for the low frequency and all *SPF*s considered, the decrease in α_w started from a threshold in the patch length characterized by $L_{patch}/h_v = 4$ (Fig. 3b). For the low frequency studied, and for all *SPF*s considered, α_w decreased with an increase in L_{patch}/h_v (Fig. 3b), without any threshold in L_{patch}/h_v. For the high frequency, f = 1.12 Hz, α_w remained constant for $L_{patch}/h_v > 20$, whereas for f = 0.5 Hz, α_w remained constant for $L_{patch}/h_v > 10$. The value of α_w reached decreased as *SPF*s increased (Fig. 3a, b).

In contrast to U_w, β_w remained constant with L_{patch}/h_v for both frequencies (1.12 Hz and 0.5 Hz) and for all *SPF*s studied (Fig. 3c and d). However, for the high frequency studied, the low vegetation densities *SPF* = 2.5%, 3.5% and 5% showed values of $\beta_w < 1$, while β_w was above 1 for *SPF* = 7.5 and 10%, with β_w increasing with SPF (Fig. 3c). Contrary to this, for the low frequency studied, $\beta_w > 1$ except for the case of SPF = 1%, for which $\beta_w = 1$ (Fig. 3d). For this frequency, β_w for *SPF* = 10% was lower than that for *SPF* = 7.5%, contrary to what had been found for the high frequency.

Following Eq. (11), two behaviours could be distinguished when considering $TKE^{1/2}$ versus$[C_{D-Patch}\frac{nd^2}{2(1-\phi)}]^{\frac{1}{3}}U_w$, and deduced by applying the non-dimensional analysis, which is shown in Fig. 4. For $[C_{D-Patch}\frac{nd^2}{2(1-\phi)}]^{\frac{1}{3}}U_w < 2$, $TKE^{1/2}$ remained constant with $[C_{D-Patch}\frac{nd^2}{2(1-\phi)}]^{\frac{1}{3}}U_w$ at a value of $TKE^{1/2} = 0.56$, while for $[C_{D-Patch}\frac{nd^2}{2(1-\phi)}]^{\frac{1}{3}}U_w > 2$, $TKE^{1/2}$ presented a linear trend versus $[C_{D-Patch}\frac{nd^2}{2(1-\phi)}]^{\frac{1}{3}}U_w$ with a slope of 0.56 (Fig. 4). The first regime (on the left in Fig. 4) corresponded to the cases where the dynamics were governed by either single stems of

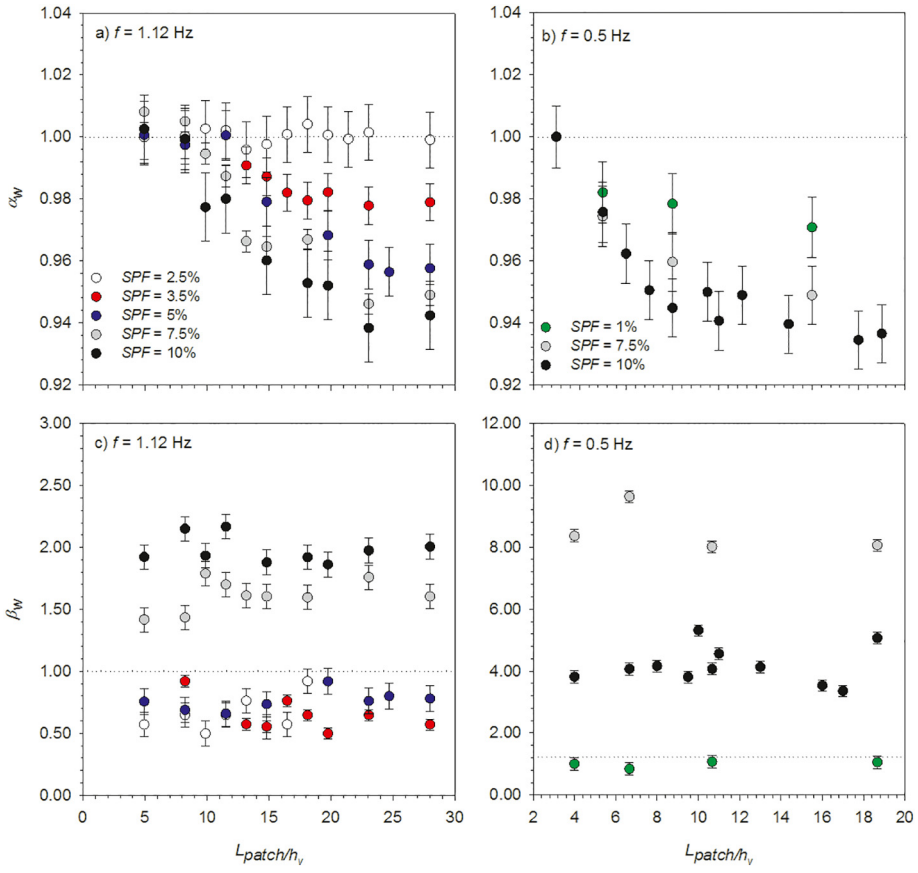

Fig. 3. Wave attenuation (α_w) versus L_{patch}/h_v for a) f = 1.12 Hz and b) f = 0.5 Hz, and *TKE* attenuation (β_w) for c) f = 1.12 Hz and d) f = 0.5 Hz at z = 4 cm, for different *SPF*s ranging from 1 to 10%.

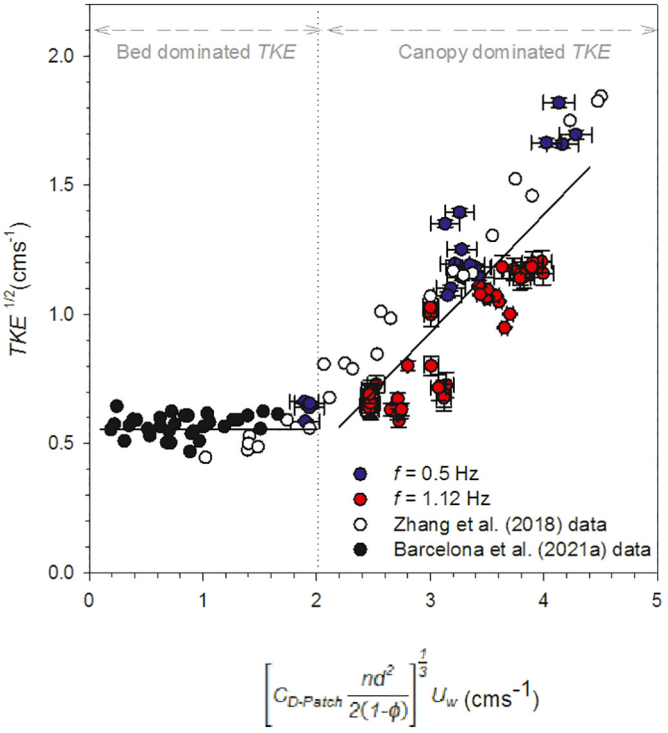

Fig. 4. Non-dimensional model for $TKE^{1/2}$ for high frequencies (red filled circles), low frequencies (blue filled circles), and Zhang et al. (2018) data (unfilled circles). H. Nepf (personal communication provided the original data from Zhang et al.'s (2018) and Barcelona et al. (2021a) data (black filled circles). The vertical dashed line represents the minimum value of $\left[C_{D-Patch}\frac{nd^2}{2(1-\phi)}\right]^{\frac{1}{3}}U_w$ that separates the different trends observed for $TKE^{1/2}$. The horizontal solid line at $TKE^{1/2} = 0.0056$ represents that for $\left[C_{D-Patch}\frac{nd^2}{2(1-\phi)}\right]^{\frac{1}{3}}U_w<2$, where $TKE^{1/2}$ remained constant. For $\left[C_{D-Patch}\frac{nd^2}{2(1-\phi)}\right]^{\frac{1}{3}}U_w> 2$ a linear tendency was found: $TKE^{1/2} = 0.47*\left[C_{D-Patch}\frac{nd^2}{2(1-\phi)}\right]^{\frac{1}{3}}U_w - 0.47$, with $R^2 = 0.73$ and 99% of confidence.

vegetation or the cases without vegetation. The second regime (on the right in Fig. 4) corresponded to the case where the dynamics were governed by the patch scale.

The transition of both regimes determines the minimum patch length $L_{patch,min}$, for which for $L_{patch} < L_{patch,\ min}$ the $TKE^{1/2}$ was independent of $[C_{D-Patch}\frac{nd^2}{2(1-\phi)}]^{\frac{1}{3}}U_w$. In this region $TKE^{1/2}$ was equal to that found for non-vegetated cases, indicating that the vegetation did not contribute to increasing the $TKE^{1/2}$. In contrast, for $L_{patch} > L_{patch,min}$ a linear trend between $TKE^{1/2}$ and $[C_{D-Patch}\frac{nd^2}{2(1-\phi)}]^{\frac{1}{3}}U_w$ was obtained. This result indicated that the experimental cases with high $L_{patch} > L_{patch,\ min}$ produced an increase in the $TKE^{1/2}$, therefore in this regime dominated by the patch scale the minimum patch length was calculated following Eq. (12), observing a dependence of the minimum patch length on L_{canopy}, canopy density and U_w, and calculated as follows:

$$L_{patch} = L_{canopy}\left[\frac{2(1-\phi)}{C_D n d^2}\left(\frac{2}{U_w}\right)^3\right]^3 \quad (13)$$

4. Discussion

In this study, the capacity of submerged patches of flexible plants to attenuate waves, in terms of their velocity and *TKE*, has been found to depend on the wave penetration within the patch and the volume occupied by the vegetation. The wave penetration was a function of the orbital excursion length scale and the plant-to-plant distance, while the volume of the vegetation patch was a function of its length and density. All of this information provides clues for determining the structural analysis of functional patches of seagrass that facilitate hydrodynamical services comparable to those of continuous seagrass meadows.

4.1. Effect of the canopy density of the patch

Here, the dynamics of functional patches that were observed to mimic the properties of a continuous vegetated canopy were characterized by the attenuation of the wave velocity with a magnitude that depended on the shoot density within the patch. This aligns with the results found previously by other authors (Gacia et al., 1999; Paul and Amos, 2011; Pujol et al., 2013b). According to the results from Ros et al. (2014) and Zhang et al. (2018), a continuous canopy also attenuates the turbulent kinetic energy generated by the bed when the wave can enter within the vegetation (i.e., $A_w/S_b < 1$, where A_w was the wave excursion length, S_b was the plant-to-plant distance between leaves, calculated as $S_b = (n_b)^{-1/2}$ (Zhang et al., 2018)). In these cases, the denser the canopy, the greater the sheltering provided. In contrast, when $A_w/S_b > 1$, the turbulent kinetic energy increases with A_w/S_b due to the interaction of the flow with the vegetation and the wakes generated by plant stems. Therefore, high canopy densities (i.e., small S_b and high A_w/S_b) result in higher *TKE* due to the production of stem wake turbulence. A range of A_w/S_b from 0.58 to 3.04 was considered in this study, covering cases with $A_w/S_b < 1$ where the *TKE* generated by the bed is attenuated and cases with $A_w/S_b > 1$ where *TKE* is generated by plant stems. In the case studied here, wave velocities at the vegetated patch ranged from 7 cm s^{-1} to 10 cm s^{-1}, resulting in stem Reynolds numbers between $Re_s = 700$ and 1000, respectively. Stem Reynolds numbers above 200 have been found to produce vortex shedding (Nepf et al., 1997) which is a source of turbulence in the system. The increase in the canopy density is expected to also produce an increase in the number of wakes generated and, in turn, an increase in the turbulent kinetic energy in the system. This aligns with the increase in the turbulent kinetic energy for the high patch densities observed in the present study.

However, this study demonstrates the contrary in that β_w remains constant with the patch size for both different *SPF*s and frequencies. Nevertheless, the results also show how patches, instead of reducing *TKE*, are capable of enhancing this energy for higher density patches (*SPF* ≤ 7.5%) for both frequencies ($f = 0.5$ and 1.12 Hz), while sparser patches attenuate the *TKE* in a range between β_w 0 to 0.5. These results agree with Zhang et al. (2018), who found that for $A_w/S_b > 1$ *TKE* was generated within the canopy. This coincides with the present study where, for both frequencies, the A_w/S_b was found to be greater than 1. These results are attributed to the increase in the number of wakes generated by the plant stems as the patch density increases which, in turn, is related to the reduction of the wave velocity (Tang et al., 2019). Folkard (2005) also found an increase of the Reynolds stress downstream of a single patch of flexible vegetation under unidirectional flow increasing with the flow velocity. Likewise, under the unidirectional flow, Tinoco and Coco (2014) also found higher *TKE* in denser canopies, thus agreeing with the results of this study even though they used emergent rigid stems.

4.2. Effect of wave velocity and frequency

Moreover, wave frequency plays a relevant and important role in wave attenuation within vegetated patches. Intermediate patch densities under oscillating flows provide greater wave attenuation for low frequencies than for high frequencies. This result is in accordance with Hansen and Reidenbach (2017) who found that lower frequencies produced a higher wave attenuation compared to higher frequencies. However, high patch densities of *SPF* = 10% produced equal wave attenuations for the two frequencies studied. These results agree with Paquier et al. (2018) who found that the attenuating capability of

waves of the patchy meadows is related to wave heights and frequencies. They also found that in the case of *Zostera noltei* Hornemann, patchy meadows are only capable of attenuating high frequency waves. These results are also in accordance with the concept that under low wave frequencies, a higher wave attenuation is produced than under high wave frequencies. Furthermore, for the low frequency case, the change from $SPF = 7.5\%$ to $SPF = 10\%$ did not produce a notable reduction in the U_w. This result might be because in high patch densities wakes are produced by stem overlap and occupy the entire region between plant stems. Therefore, a further increase in vegetation might not produce a subsequent increase in the turbulent kinetic energy locally. This result is in accordance with the definition of a patch of vegetation as described by Schoelynck et al. (2018).

4.3. Effect of the patch length scale

This study also demonstrates that the patch size plays a crucial role in determining the hydrodynamics within the vegetated patches. For low wave frequencies, the wave attenuation at the centre of the patch depended on its shoot density. These results may be related to the studies from Zong and Nepf (2010) and Devi and Kumar (2016), who found a lower linear velocity attenuation through sparse patches than through dense patches. In contrast, for high wave frequencies, small patches with $L_{patch} < 6h_v$, do not provide any reduction in the wave velocity compared with the without-plants case, whereas patches of $L_{patch} > 6h_v$ reduce the wave velocity as the canopy density increases. These results align with those from Licci et al. (2019), who found that the effect of small patches ($L_{patch}/h_v > 9$) of *Callitriche platycarpa,* Kütz in the attenuation of the linear velocity was little or negligible, while larger patches induced significant modifications in the linear velocity.

4.4. Patch length-scale thresholds

The non-dimensional model for the $TKE^{1/2}$ indicated that $TKE^{1/2}$ remains nearly constant for $[C_{D-Patch}\frac{nd^2}{2(1-\phi)}]^{\frac{1}{3}}U_w < 2$. Low values of $[C_{D-Patch}\frac{nd^2}{2(1-\phi)}]^{\frac{1}{3}}U_w$ can hold for both, low wave frequencies, sparse patches, or small patches. Therefore, a low volume of vegetation produces a constant value of $TKE^{1/2} = 0.56$, which is the same value obtained for the non-vegetated cases, hence the *TKE* source is generated by the bed friction. This threshold means that the minimum patch size required for a certain patch density and under certain hydrodynamical conditions to be dynamically functional as a continuous canopy can be determined. Conversely, it also means that the minimum density required for a certain patch length to play a role as a patch (instead of a non-vegetated case) can be determined, increasing the *TKE* by the interaction between the wave and the plants. That said, the results presented here not only show this, but also that the behaviour of a patch also depends on the hydrodynamics i.e., wave frequency and velocity. For cases of $[C_{D-Patch}\frac{nd^2}{2(1-\phi)}]^{\frac{1}{3}}U_w > 2$, the $TKE^{1/2}$ increased with $[C_{D-Patch}\frac{nd^2}{2(1-\phi)}]^{\frac{1}{3}}U_w$. It is interesting to notice that a certain patch with a certain canopy density might not generate *TKE* for low U_w i.e., $[C_{D-Patch}\frac{nd^2}{2(1-\phi)}]^{\frac{1}{3}}U_w < 2$, but after an increase in U_w it can interact with the wave field, producing *TKE* i.e., $[C_{D-Patch}\frac{nd^2}{2(1-\phi)}]^{\frac{1}{3}}U_w > 2$.

4.5. Management strategies

From a hydrodynamical point of view, a minimum patch size is required for the patch to interact with the wave flow and move from of a regime dominated by either the single stem scale or the non-vegetated case towards a regime dominated by the canopy. From this point of view, this study provides management strategies for potential successful seagrass meadow restoration. West et al. (1990) studied the survival of *Zostera muelleri* subsp., *capricorni* (Ascherson) S.W.L. Jacobs, and *Posidonia australis*, J.D. Hooker, transplants. For *P. australis* canopies, single shoots, or clumps of 2–3 shoots were transplanted, while for *Z. mulleri* subsp. *capricorni* about 20–30 shoots were used as transplanted units. The transplants were monitored and only very few survived under high energetic events, indicating that the parametrization of the transplanted shoots may have been incomplete. In addition, Infantes et al. (2009) reported that $U_w > 38$–42 cm·s^{-1} caused a decrease in the cover of the *Posidonia oceanica* meadows meaning that, for these velocities, the generation of *TKE* within the patch will become extremely high and will produce a sufficient level of seabed erosion to potentially cause irreversible plant loss. Therefore, hydrodynamics need to be included in the parameterization for future seagrass restoration projects.

Furthermore, Stipek et al. (2020) demonstrated that the mortality rate of seagrass patches depended on the size of the patch, with small patches (<50 m^2, $L_{patch} < 7.07$ m) undergoing a high annual mortality rate (of 57%) compared to the lower mortality rate (<5%) found for larger patches. If a mean leaf length of 0.8 m is considered (Gruber and Kemp, 2010), assuming that leaf would bend the same percentage like that in the current study for a typical frequency of 0.5 Hz ($h_v =$ 10.5 cm for a leaf length of 14 cm, 75% of the leaf length), h_v in the field would be 0.6 m. Then their small patches would correspond to lengths equal to or smaller than $L_{patch} = 7.07$ m $= 11.78\, h_v$. This finding aligns with the transition observed in this study, where for $L_{patch} > 10h_v$ and for typical ocean waves of $f = 0.5$ Hz, α_w remains constant, indicating that the patch behaves like a continuous canopy. In contrast, for $L_{patch} < 10h_v$, α_w increases towards the value for the non-vegetated case as L_{patch} decreases.

By applying the model found in the current study, the behaviour of patches found in natural seagrass meadows under different hydrodynamic conditions can be determined. In fact, two behaviours have been observed: one where plants do not interact with the wave field and another where they do, thus generating *TKE*. Considering the findings of the present study, the results found by Barcelona et al. (2021b) for Cala Aiguablava and Cala Vigatà - two fragmented meadows found on the northeast Spanish coast - have been analyzed. The meadow in Cala Aiguablava presents 66% fragmentation, with the smallest patch lengths being 0.64 m and the largest 8.06 m. The plant density oscillated between 449 and 105 plants·m^{-2} between the 2 years studied. Meanwhile, the meadow in Cala Vigatà presents 22% fragmentation, with the smallest patches being 5.23 m long and the largest 24.82 m. The plant density in Cala Vigatà oscillated between 353 and 119 plants·m^{-2} (Barcelona et al., 2021a). These meadows are categorized as a medium patch vegetation and a perforated meadow, respectively, following the classification by Sleeman et al., 2005, see Barcelona et al., 2021b). Using the model proposed in this study, the minimum patch size required for the vegetation to produce *TKE* for these bays has been determined by considering the typical wave frequency of the Mediterranean Sea (0.5 Hz) and a range of wave velocities between 0.5 and 30 cm·s^{-1}. For $h_v = 0.6$ m, $L_{canopy} = 10h_v$ would be $L_{canopy} = 6$ m For the high canopy densities and for $U_w < 5$ cm·s^{-1}, the minimum patch size required to produce *TKE* was $L_{patch} > 225$ m for Cala Aiguablava and $L_{patch} > 963$ m for Cala Vigatà, indicating unfavourable conditions for small patches under these wave velocities. In contrast, for $U_w > 5$ cm·s^{-1}, the minimum patch size required decreased to very low values in both bays (<0.06 m in Cala Aiguablava and <0.25 m in Cala Vigatà). In contrast, for low canopy densities and $U_w > 5$ cm·s^{-1} the minimum patch size was $L_{patch} = 36$ m for Cala Aiguablava and 24 m for Cala Vigatà, due to the different canopy densities in both meadows. Therefore, patches smaller than this threshold would be threatened. In the low-density canopy cases and $U_w < 5$ cm·s^{-1}, the minimum patch size required would be 194,606 m for Cala Aiguablava and 125,720 m for Cala Vigatà. Under such conditions all patches would be threatened. These results align with those found by Pujol et al. (2019) for oxygen transport

through the diffusive boundary layer (DBL). They found that by increasing the flow velocity, the DBL becomes thinner and the gas exchange by the plant is enhanced. They also found that for $U_w < 6\ cm \cdot s^{-1}$, the gas exchange through the DBL is reduced. This result is close to the velocity limit found for the two bays analyzed in the present study, where $U_w > 5\ cm \cdot s^{-1}$ produce plant-wave interactions, generating *TKE* and enhancing the particle mixing.

5. Conclusions

This study demonstrates that patches of seagrasses can respond to waves by adhering to two hydrodynamic behaviours that depend on wave velocity. The first behaviour corresponds to low wave velocities where plants do not interact with waves. In this case, plants dissipate the near-bed generated turbulence. The second behaviour corresponds to moderate wave velocities where plants interact with waves through the production of *TKE*. The two behaviours ultimately depend on the density of the canopy and the length of the patch. High canopy densities are expected to produce greater *TKE* than low canopy densities. In addition, the production of *TKE* holds for small patches under moderate wave velocities or, conversely, for low wave velocities acting on large canopy areas. In such cases, the production of *TKE* is guaranteed, providing vegetated patches with functional dynamics to optimize the ecosystems services they provide. For patches with length dimensions greater than the minimum patch scale, the production of *TKE* by the plants in the patch might enhance the gas exchange in plant leaves, which will favour patch resilience under wave activity. In contrast, the resilience and resistance of seagrass canopies undergoing patchiness might be compromised when vegetated patches do not interact with the flow, since their length scale is lower than the required minimum patch scale that provide patch/flow interaction.

CRediT authorship contribution statement

Aina Barcelona: Methodology, Investigation, Formal analysis, Data curation, Writing – original draft. **Carolyn Oldham:** Methodology, Writing – review & editing. **Jordi Colomer:** Conceptualization, Methodology, Data curation, Writing – review & editing. **Teresa Serra:** Conceptualization, Methodology, Data curation, Writing – review & editing, Supervision.

Declaration of competing interest

The authors declare that they have no known competing financial interests or personal relationships that could have appeared to influence the work reported in this paper.

Acknowledgements

This research was funded by the “Ministerio de Economía, Industria y Competitividad” of the Spanish Government through the grant CGL2017-86515-P. Aina Barcelona was funded by the pre-doctoral grant 2020 FI SDUR 00043 by the “Generalitat de Catalunya”.

References

Abadie, A., Lejeune, P., Pergent, G., Gobert, S., 2016. From mechanical to chemical impact of anchoring in seagrasses: the premises of anthropogenic patch generation in *Posidonia oceanica* meadows. Mar.Pollut.Bull. 109, 61–71. https://doi.org/10.1016/j.marpolbul.2016.06.022.

Bacci, T., Rende, F.S., Scardi, M., 2017. Shoot micro distribution patterns in the Mediterranean seagrass Posidonia oceanica. Mar.Biol. 164, 85. https://doi.org/10.1007/s00227-017-3121-1.

Barcelona, A., Colomer, J., Soler, M., Gracias, N., Serra, T., 2021a. Meadow fragmentation influences Posidonia oceanica density at the edge of nearby gaps. Estuar. Coast. Shelf. S. 249, 107106. https://doi.org/10.1016/j.ecss.2020.107106.

Barcelona, A., Oldham, C., Colomer, J., Garcia-Orellana, J., Serra, T., 2021b. Particle capture by seagrass canopies under an oscillatory flow. In Revision in Coastal Engineering.

Bouma, T.J., van Duren, L.A., Temmerman, S., Claverie, T., Blanco-Garcia, A., Ysebaert, T., Herman, P.M.J., 2007. Spatial flow and sedimentation patterns within patches of epibenthic structures: combining field, flume and modelling experiments. Cont. Shelf Res. 27, 1020–1045. https://doi.org/10.1016/j.csr.2005.12.019.

Carr, J., D'Odorico, P., McGlathery, K., Wiberg, P., 2010. Stability and biostability of seagrass ecosystems in shallow coastal lagoons: role of feedbacks with sediment resuspension and light attenuation. J Geophys Res-Biogeo 115, 1–14. https://doi.org/10.1029/2009JG001103.

Colomer, J., Soler, M., Serra, T., Casamitjana, X., Oldham, C., 2017. Impact of anthropogenically created canopy gaps on wave attenuation in a Posidonia oceanica seagrass meadow. Mar. Ecol. Prog. Ser. 569, 103–116. https://doi.org/10.3354/meps12090.

Devi, T.B., Kumar, B., 2016. Experimentation on submerged flow over flexible vegetation patches with downward seepage. Ecol. Eng. 91, 158–168. https://doi.org/10.1016/j.ecoleng.2016.02.045.

El Allaoui, N., Serra, T., Colomer, J., Soler, M., Casamitjana, X., Oldham, C., 2016. Interactions between fragmented seagrass canopies and the local hydrodynamics. PLoS One 11 (5), e0156264. https://doi.org/10.1371/journal.pone.0156264.

Folkard, A.M., 2005. Hydrodynamics of model *Posidonia oceanica* patches in shallow water. Limnol. Oceanogr. 50 (5), 1592–1600. https://doi.org/10.4319/lo.2005.50.5.1592.

Fourqurean, J.W., Duarte, C.M., Kennedy, H., Marbà, N., Holmer, M., Mateo, M.A., Apostolaki, E.T., Kendrick, G.A., Krause-Jensen, D., McGathery, K.J., Serrano, O., 2012. Seagrass ecosystems as a globally significant carbon stock. Nat. Geosci. 5 (7), 505–509. https://doi.org/10.1038/ngeo1477.

Gacia, E., Granata, T.C., Duarte, C.M., 1999. An approach to measurement of particle flux and sediment retention within seagrass (*Posidonia oceanica*) meadows. Aquat. Bot. 65, 255–268.

Gera, A., Pagès, J., Romero, J., Alcoverro, T., 2013. Combined effects of fragmentation and herbivory on *Posidonia oceanica* seagrass ecosystems. J. Ecol. 101, 1053–1061. https://doi.org/10.1111/1365-2745.12109.

Ghisalberti, M., Nepf, H., 2002. Mixing layers and coherent structures in vegetated aquatic flows. J. Geophys. Res. 107, C23011. https://doi.org/10.1029/2001JC000871.

Gilby, B.L., Olds, A.D., Duncan, C.K., Ortodossi, N.L., Henderson, C.J., Schlacher, T.A., 2020. Identifying restoration hotspots that deliver multiple ecological benefits. Restor. Ecol. 28 (1), 222–232. https://doi.org/10.1111/rec.13046.

Goring, D.G., Nikora, V.I., 2002. Despiking acoustinc Doppler velocimeter data. J. Hydraul. Eng. 128 (1), 117–126. https://doi.org/10.1061/(ASCE)0733-9429(2002)128:1(117).

Granata, T., Serra, T., Colomer, J., Casamitjana, X., Duarte, C.M., Gacia, E., 2001. Flow and particle distribution in a nearshore seagrass meadow before and after a storm. Mar. Ecol. Prog. Ser. 218, 95–106. https://doi.org/10.3354/meps218095.

Grech, A., Chartrand-Miller, K., Erftemeijer, P., Fonseca, M., McKenzie, L., Rasheed, M., Taylor, H., Coles, R., 2012. A comparison of threats, vulnerabilities and management approaches in global seagrass bioregions. Environ. Res. Lett. 7 (2), 024006. https://doi.org/10.1088/1748-9326/7/2/024006.

Gruber, R.K., Kemp, W.M., 2010. Feedback effects in a coastal canopy-forming submersed plant bed. Limnol. Oceanogr. 55 (6), 2285–2298. https://doi.org/10.4319/lo.2010.55.6.2285.

Hansen, J.C.R., Reidenbach, M.A., 2017. Turbulent mixing and fluid transport within Florida Bay seagrass meadows. Adv. Water Resour. 108, 205–215. https://doi.org/10.1016/j.advwaters.2017.08.001.

Hughes, A.R., Williams, S.L., Duarte, C.M., Heck Jr., K.L., Waycott, M., 2009. Associations of concern: declining seagrasses and threatened dependent species. Front. Ecol. Environ. 7 (5), 242–246. https://doi.org/10.1890/080041.

Infantes, E., Terrados, J., Orfila, A., Cañellas, B., Álvarez-Ellacuria, A., 2009. Wave energy and the upper depth limit distribution of *Posidonia oceanica*. Bot. Mar. 52, 419–427. https://doi.org/10.1515/BOT.2009.050.

Kupsky, B.G., Dornbush, M.E., 2019. Experimental test of abiotic and biotic factors driving restoration success of Vallisneria americana in the Lower Bay of Green Bay. J. Great Lakes Res. 45, 340–349. https://doi.org/10.1016/j.jglr.2019.01.006.

Li, W., Wang, D., Jiao, J., Yang, K., 2019. Effects of vegetation patch density on flow velocity characteristics in an open channel. J. Hydrodyn. 31 (5), 1052–1059. https://doi.org/10.1007/s42241-018-0086-6.

Licci, S., Nepf, H., Delome, C., Marmonier, P., Bouma, T.j., Puijalon, S., 2019. The role of patch size in ecosystem engineering capacity: a case study of aquatic vegetation. Aquat. Sci. 81 (3), 41. https://doi.org/10.1007/s00027-019-0635-2.

Lowe, R.J., Koseff, J.R., Monismith, S.G., 2005. Oscillatory flow through submerged canopies: 2. Canopy mass transfer. J. Geophys. Res. 110, C10017. https://doi.org/10.1029/2004JC002789.

Luhar, M., Coutu, S., Infantes, E., Fox, S., Nepf, H., 2010. Wave-induced velocities inside a model seagrass bed. J. Geophys. Res. 115, C12005. https://doi.org/10.1029/2010JC006345.

Metz, J.L., Harris, R.J., Arrington, D.A., 2020. Seasonal occurrence patterns of seagrass should influence resource assessment and management decisions: a case study in the Indian River Lagoon and Loxahatchee River Estuary, Florida. Reg. Stud. Mar. Sci. 34, 101093. https://doi.org/10.1016/j.rsma.2020.101093.

Montefalcone, M., 2009. Ecosystem health assessment using Mediterranean seagrass *Posidonia oceanica*. Ecol. Indic. 9, 595–604. https://doi.org/10.1016/j.ecolinf.2008.09.013.

Nepf, H.M., Sullivan, A., Zavistoski, R.A., 1997. A model for diffusion within emergent vegetation. Limnol. Oceanogr. 42 (8), 1735–1745. https://doi.org/10.4319/lo.1997.42.8.1735.

Newell, R.I.E., Koch, E.W., 2004. Modeling seagrass density and distribution in response to changes in turbidity stemming from bivalve filtration and seagrass sediment stabilization. Estuaries 27, 793–806. https://doi.org/10.1007/BF0912041.

Paling, E.I., van Keulen, M., Wheeler, K.D., Phillips, J., Dyhrberg, R., 2003. Influence of 593 spacing on mechanically transplanted seagrass survival in a high wave energy

regime. 594. Restor. Ecol. 11 (1), 5–61. https://doi.org/10.1046/j.1526-100X.2003.00072.x.

Paquier, A., Meulé, S., Anthony, E.J., Larroudé, P., Bernard, G., 2018. Wind-induced hydrodynamics interactions with aquatic vegetation in a fetch-limited setting: implications for coastal sedimentation and protection. Estuar. Coasts 42, 688–707. https://doi.org/10.1007/s12237-018-00487-w.

Paul, M., Amos, C.L., 2011. Spatial and seasonal variation in wave attenuation over *Zostera noltii*. J. Geophys. Res. 116, C08019. https://doi.org/10.1029/2010JC006797.

Pujol, D., Casamitjana, X., Serra, T., Colomer, J., 2013a. Canopy-scale turbulence under oscillatory flow. Cont. Shelf Res. 66, 9–18. https://doi.org/10.1016/j.csr.2013.06.012.

Pujol, D., Serra, T., Colomer, J., Casamitjana, X., 2013b. Flow structure in canopy models dominated by progressive waves. J. Hydrol. 486, 281–292. https://doi.org/10.1016/j.jhydrol.2013.01.024.

Pujol, D., Abdolahpour, M., Lavery, P.S., McMahon, K., Oldham, C., 2019. Flow velocity and nutrient uptake in marine canopies. Mar. Ecol. Prog. Ser. 622, 17–30. https://doi.org/10.3354/meps12987.

Robbins, B.D., Bell, S.S., 1994. Seagrass landscapes: a terrestrial approach to the marine subtidal environment. Trends Ecol. Evol. 9 (8), 301–304. https://doi.org/10.1016/0169-5347(94)90041-8.

Ros, À., Colomer, J., Serra, T., Pujol, D., Soler, M., Casamitjana, X., 2014. Experimental observations on sediment resuspension within submerged model canopies under oscillatory flow. Cont. Shelf Res. 91, 220–231. https://doi.org/10.1016/j.csr.2014.10.004.

Schoelynck, J., Creëlle, S., Buis, K., De Mulder, T., Emsens, W.J., Hein, T., Meire, D., Meire, P., Okrusko, T., Preiner, S., González, R.-R., Silinski, A., Temmerman, S., Troch, P., Van Oyen, T., Verschoren, V., Visser, F., Wang, C., Wolters, J.W., Folkard, A., 2018. What is a macrophyte patch? Patch identification in aquatic ecosystems and guidelines for consistent delineation. Ecohydrol.Hydrobiol. 18, 1–9. https://doi.org/10.1016/j.ecohyd.2017.10.005.

Serra, T., Oldham, C., Colomer, J., 2018. Local hydrodynamics at edges of marine canopies under oscillatory flows. PLoS One 13 (8), e0201737. https://doi.org/10.1371/journal.pone.0201737.

Sleeman, J.C., Kendrick, G.A., Boggs, G.S., Hegge, B.J., 2005. Measuring fragmentation of seagrass landscapes: which indices are most appropriate for detecting change? Mar.Freshwater.Res. 58, 851–864. https://doi.org/10.1071/MF04300.

Stankovic, M., Kaewsrikhaw, R., Rattanachot, E., Prathep, A., 2019. Modeling of suitable habitat of small-scale seagrass restoration in tropical ecosystems. Estuar. Coast. Shelf. S. 231, 106465. https://doi.org/10.1016/j.ecss.2019.106465.

Stipek, C., Santos, R., Barcock, E., Lirman, D., 2020. Modelling the resilience of seagrass communities exposed to pulsed freshwater discharges: a seascape approach. PLoS One 15 (2), e0229147. https://doi.org/10.1371/journal.pone.0229147.

Tang, C., Lei, J., Nepf, H.M., 2019. Impact of vegetation-generated turbulence on the critical, near-bed, wave-velocity for sediment resuspension. Water Resour. Res. 55, 5904–5917. https://doi.org/10.1029/2018WR024335.

Tanner, J.E., 2003. Patch shape and orientation influences on seagrass epifauna are mediated by dispersal abilities. Oikos 100 (3), 517–524. https://doi.org/10.1034/j.1600-0706.2003.12060.x.

Tinoco, R.O., Coco, G., 2014. Observation of the effect of emergent vegetation on sediment resuspension under unidirectional currents and waves. Earth. Surf. Dynam. 2, 83–96. https://doi.org/10.5194/esurf-2-83-2014.

Unsworth, R.K.F., McKenzie, L.J., Collier, C.J., Cullen-Unsworth, L.C., Duarte, C.M., Eklöf, J.S., Jarvis, J.C., Jones, B.L., Nordlund, L.M., 2018. Global challenges for seagrass conservation. Ambio 48 (8), 801–815. https://doi.org/10.1007/s13280-018-1115-y.

van Katwijk, M.M., Bos, A.R., Hermus, D.C.R., Suykerbuyk, W., 2010. Sediment modification by seagrass beds: Muddification and sandification induced by plant cover and environmental conditions. Estuar. Coast. Shelf. S. 89, 175–181. https://doi.org/10.1016/j.ecss.2010.06.008.

van Katwijk, M.M., Thorhaug, A., Marbà, N., Orth, R.J., Guarte, C.M., Kendrick, G.A., Althuizen, I.H.J., Balestri, E., Bernard, G., Cambridge, M.L., Cunha, A., Durance, C., Giesen, W., Han, Q., Hosokawa, S., Kiswara, W., Komatsu, T., Lardicci, C., Lee, K., Meinesz, A., Nakaoka, M., O'Brien, K.R., Paling, E.I., Pickerell, C., Ransijn, A.M.A., Verduin, J.J., 2016. Global analysis of seagrass restoration: the importance of large-scale planting. J. Appl. Ecol. 53, 567–578. https://doi.org/10.1111/1365-2664.12562.

Waycott, M., Duarte, C.M., Carruthers, T.J.B., Orth, R.J., Dennison, W.C., Olyarnik, S., Calladine, A., Fourqurean, J.W., Heck, K.L., Hughes, A.R., Kendrick, G.A., Kenworthy, W.J., Short, F.T., Williams, S.L., 2009. Accelerating loss of seagrasses across the globe threatens coastal ecosystems. PNAS 106 (30), 12377–12381. https://doi.org/10.1073/pnas.0905620106.

West, R.J., Jacobs, N.E., Roberts, D.E., 1990. Experimental transplanting of seagrasses in Botany Bay, Australia. Mar. Pollut. Bull. 21 (4), 197–203 (doi: 0025-326X/90).

Zhang, Y., Tang, C., Nepf, H., 2018. Turbulent kinetic energy in submerged model canopies under oscillatory flow. Water Resour. Res. 54, 1734–1750. https://doi.org/10.1002/2017WR021732.

Zong, L., Nepf, H., 2010. Flow and deposition in and around a finite patch of vegetation. Geomorphology 116, 363–372. https://doi.org/10.1016/j.geomorph.2009.11.020.